Multiphoton microscopy of cleared mouse organs

Sonia G. Parra
Thomas H. Chia
Joseph P. Zinter
Michael J. Levene
Yale University
Department of Biomedical Engineering
New Haven, Connecticut 06520

Abstract. Typical imaging depths with multiphoton microscopy (MPM) are limited to less than 300 μm in many tissues due to light scattering. Optical clearing significantly reduces light scattering by replacing water in the organ tissue with a fluid having a similar index of refraction to that of proteins. We demonstrate MPM of intact, fixed, cleared mouse organs with penetration depths and fields of view in excess of 2 mm. MPM enables the creation of large 3-D data sets with flexibility in pixel format and ready access to intrinsic fluorescence and second-harmonic generation. We present high-resolution images and 3-D image stacks of the brain, small intestine, large intestine, kidney, lung, and testicle with image sizes as large as 4096 $\times$ 4096 pixels. © *2010 Society of Photo-Optical Instrumentation Engineers.* [DOI: 10.1117/1.3454391]

Keywords: fluorescence; multiphoton microscopy; cleared; intrinsic; organ; mouse; second harmonic; histology.

Paper 10151R received Mar. 23, 2010; revised manuscript received Apr. 13, 2010; accepted for publication Apr. 15, 2010; published online Jun. 21, 2010.

1 Introduction

There has been renewed interest in the use of optical clearing[1,2] of fixed tissue by dehydration followed by immersion in a solution of 1:2 benzyl alcohol to benzyl benzoate (BABB).[3–5] Recent work includes imaging thick specimens using side-on illumination with a "sheet" of light, sometimes referred to as "ultramicroscopy,"[6] and the related technique "selective plane illumination microscopy."[7] These methods have been shown to produce images of extrinsic fluorophores, including green fluorescent proteins and Cy3, as well as intrinsic fluorescence from small samples. However, the size of tissue that can be effectively imaged is limited both by significant residual scattering due to imperfect clearing and by the trade-off between the thickness of the light sheet and limits on the field of view due to diffraction. For example, for a light sheet of thickness ~6 to 8 μm, the field of view would be limited to ~660 μm due to diffraction alone.[7] In addition, the pixel dimensions and maximum number of pixels are fixed by the choice of CCD camera.

Multiphoton microscopy (MPM)[8,9] of cleared tissues offers several advantages:

- MPM is far more tolerant of residual scattering and is therefore not significantly limited in imaging depth.
- Because MPM is a scanning technique, the image size is limited only by the objective lens used, and pixel dimensions and total pixel number can be chosen at will to optimize image quality.
- MPM can access nonlinear signals such as second-harmonic generation that one-photon techniques cannot.
- MPM is well-suited to exciting a wide range of intrinsic fluorescence[10] that would otherwise require more highly scattering UV excitation.

The latter two points are particularly relevant to the development of 3-D histology, in which intrinsic fluorescence and second harmonic signals from large (>1 mm) portions of unstained biopsy tissue are imaged with high resolution prior to traditional mounting, slicing, and staining in order to form a "virtual" biopsy consisting of a very large 3-D data set that can be manipulated at will by a pathologist. Previously, whole organ images using MPM were produced by combining MPM's optical sectioning capability with the sequential automated slicing[11] or ablation[12] of fixed tissue specimens. On completion, there is no tissue left for further whole organ imaging and histological study. Optical clearing negates the necessity to use manual slicing to achieve whole organ images and leaves the tissue intact for repeated imaging or for traditional histological preparations.

2 Materials and Methods

Organ samples were obtained from FVB and C57 black 6 mice. Each mouse was anesthetized with an intraperitoneal injection of ketamine/xylazine (100 mg/kg: 10 mg/kg) and then restrained to the surgical bed by adhering each limb so that the mouse was in the supine position, exposing its chest for surgical incision. An incision was made below the xyphoid process, and the heart was exposed by cutting along the base and then through the center of the rib cage. A 23-g needle was then inserted into the left ventricle of the heart and perfused with 4 °C Delbecco's phosphate buffered saline (PBS; pH 7.0) until only PBS was observed exiting a puncture in the right atrium. This was immediately followed with a perfusion of a 4% paraformaldehyde (PFA) solution (10 g PFA/250 mL PBS) at 4 °C until the mouse's body became noticeably stiff and rigid. The kidney, lungs, brain, testicle, and intestine were then dissected out and placed in individual glass vials, where they were submerged in 4% PFA to allow for sufficient fixa-

Address all correspondence to Michael J. Levene, Department of Biomedical Engineering, Yale University, New Haven, CT 06520. Tel: 203.432.4264; Fax: 203.432.0030; E-mail: Michael.Levene@Yale.edu

1083-3668/2010/15(3)/036017/5/$25.00 © 2010 SPIE

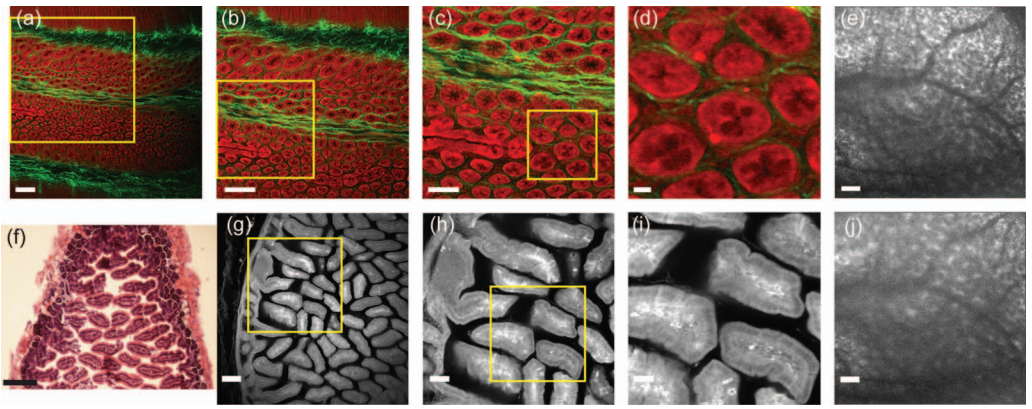

Fig. 1 Images of mouse intestine. (a) Intrinsic fluorescence (red) and second-harmonic generation from collagen (green) in the small intestine imaged 300 μm below the surface (Scale bar=100 μm). (b) to (d) Digital zooms of the original, 4096×4096 image in (a) as marked by yellow boxes. [scale bars=100 μm, 50 μm, and 10 μm for (b) to (d), respectively.] (f) Histological section of small intestine with H&E staining prepared after clearing process. (Scale bar=200 μm.) (g) Intrinsic fluorescence image of large intestine imaged 1.3 mm from the surface. (Scale bar =100 μm.) (h) and (i) Digital zooms of original 4096×4096 image in (g) as marked by yellow boxes. [Scale bar=50 μm and 25 μm in (h) and (i), respectively.] (e) and (j) Images of small intestine from noncleared tissue at depths of 50 μm (e) and 100 μm (j) showed less detail and have limited imaging depth. (Scale bars=100 μm.)

tion. The vials were then placed on a hot plate at 37 °C for 4 h, then sealed, and left overnight at 4 °C. After approximately 12 h, each organ was rinsed twice with PBS at room temperature and dehydrated using a graded methanol series (50%, 70%, 95%, and twice at 100%) with each step lasting 30 min. This was accomplished by draining each vial of solution and immediately replacing it with the next methanol solution in the series.

Organs were cleared using a solution of 1:2 benzyl alcohol to benzyl benzoate (BABB). BABB was used because it has demonstrated the most complete clearing of tissues. After the dehydration steps were completed, the organs were each placed in a 1:1 solution of methanol:BABB for 4 h. The 1:1 solution was then drained away and replaced by a 100% BABB solution. The organs were allowed to clear overnight at room temperature.

Images were taken using a custom-built multiphoton microscope that incorporated a Mai Tai titanium sapphire laser adjustable between a 710-nm to 990-nm excitation wavelength. The excitation wavelength used to generate autofluorescence was 740 nm. Appropriate choice of microscope objective must be made to simultaneously maximize both the field of view and the resolution of the system, while also compensating for spherical aberrations induced by the sample and clearing solution. We used a 5× magnification macro lens with 0.5 numerical aperture (NA) that included a correction collar for up to 3 mm of water (AZ Plan Fluor, Nikon Corp., Tokyo, Japan) to capture the reflected intrinsic fluorescence (unless otherwise noted). Because the refractive index of the BABB solution is higher than that of water, the correction collar setting was optimized by visual inspection of image quality without reference to the water-calibrated settings of the lens. The emitted fluorescence was collected from the wavelengths of 420 to 500 nm. The second-harmonic generation (360 to 380 nm) was captured using an F1 lens or an Olympus 40× objective (LUCPlanFL N, NA=0.6). Both spectra were collected using photomultiplier tubes (PMTs; HC-125-02, Hamamatsu, Bridgewater, New Jersey) and processed using a modified version ScanImage software[13] at a resolution of 1024×1024 or 4096×4096 pixels at a scan rate of 4 to 8 ms per line.

The optically cleared tissue was first taken out of its glass vial and placed on a lab wipe to absorb the excess clearing solution (1:2 BABB) from the surface of the tissue. A small dot of cyanoacrylate was then dabbed onto the bottom of a Petri dish and the tissue sample placed on top. The sample was left for 5 min in order for the tissue to securely adhere to the bottom of the dish. Excess 1:2 BABB solution was then poured into the Petri dish until the sample was fully submerged. Images were acquired from the submerged tissue sample.

The intrinsic fluorescence and second-harmonic signals were separated into two channels. The two channels were later merged together to create one image in which the collected intrinsic fluorescence (red) and the second-harmonic signal (green) could be seen simultaneously. A z-stack was produced by taking 1024×1024 pixel images all the way through the organ in 5- 10-μm steps in excess of 2 mm beneath the tissue surface. Single high-resolution images at 4096×4096 pixels were created by merging the corresponding intrinsic and second-harmonic image signals together.

A fiber optic spectrometer (USB2000, Ocean Optics, Dunedin, Florida) was connected to the two-photon microscope and used to analyze the intrinsic fluorescence spectra of optically cleared lungs, intestine, and brain. The epifluorescence generated by the samples was collected using a combination of emission filters by switching between a 460/80 and 575/150 filter. Each sample was prepared as described earlier, and the fluorescence was generated using an excitation wavelength of 740 nm.

3 Results and Discussion

Figures 1(a)–1(d) show images of the small intestine 300 μm below the organ's surface, with intrinsic fluorescence in red and SHG from collagen in green, revealing individual villi

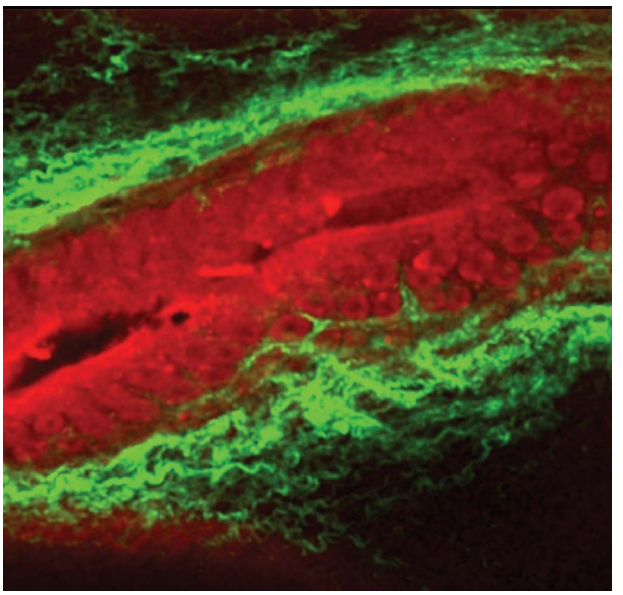

Video 1 Z-stack of the entire 1.7-mm thickness of the small intestine. Each image is a 5-μm step in the z direction. Intrinsic fluorescence is in red, and second-harmonic generation from collagen is in green (QuickTime, 1.7 MB). [URL: http://dx.doi.org/10.1117/1.3454391.1]. (Color online only.)

and surrounding collagen. The large format of 4096 $\times$4096 pixels in the original 1-mm field of view in Fig. 1(a) enabled successive zooms to reveal increasing levels of detail. A z-stack of the entire 1.7-mm thickness of the intestine with 5-μm steps was taken using a 4$\times$, 0.28 NA objective (XLFluor4x/340, Olympus America, Inc., Center Valley, Pennsylvania; Video 1). In this case, the lower-NA lens was used to maximize field of view and because a smaller image size (1024$\times$1024 pixels) was used for smaller file size. After imaging, conventional histological sections with hematoxylin and eosin (H&E) staining were prepared [see Fig. 1(f)], demonstrating that the clearing process does not interfere with histological staining. Figures 1(g)–1(i) show intrinsic fluorescence images of the large intestine, 1.3 mm below the surface, displaying morphological details similar to the H&E stained section. Note that there is no significant loss of resolution in Figs. 1(g)–1(i) compared to Figs. 1(a)–1(d), despite the former being taken 1 mm deeper into tissue. For comparison, Figs. 1(e) and 1(j) show images taken from fixed small intestine that was not cleared at 50 μm and 100 μm below the organ surface, respectively. We could not obtain images deeper than $\sim$100 μm in any noncleared organs, and in most cases, we could not obtain useful images at depths greater than 75 μm. Images from noncleared organs at any depth showed significantly less detail and generally poorer image quality than those from cleared organs.

Figure 2 is a 2$\times$2 mm image of the lung collected 1.4 mm beneath the surface. The collagen fibers (green) outlining the bronchiole pathways are clearly defined within the elastin (red) that composes the majority of the lung tissue. Green striations marking the collagen in bronchioles are particularly clear in Figs. 2(b) and 2(c), while individual alveoli are well defined in Figs. 2(c) and 2(d). Taking a z-stack in 5-μm steps allowed for imaging of 2.2 mm of the lung (Video 2).

Images of testes in Figs. 3(a)–3(d) show seminiferous tubules ($\sim$1.4 mm deep) surrounded by a supportive framework of collagen. The transition from the periphery to the center of the tubules of spermatocytes maturing to spermatids and spermatozoa are visible in Figs. 3(c) and 3(d). Figures 3(e)–3(h) are images taken from the medulla of the kidney 1.1 mm beneath the surface of cortex. The successive zooms from the original 1-mm field of view reveal the inner networking of nephrons with cellular detail in Figs. 3(g) and 3(h).

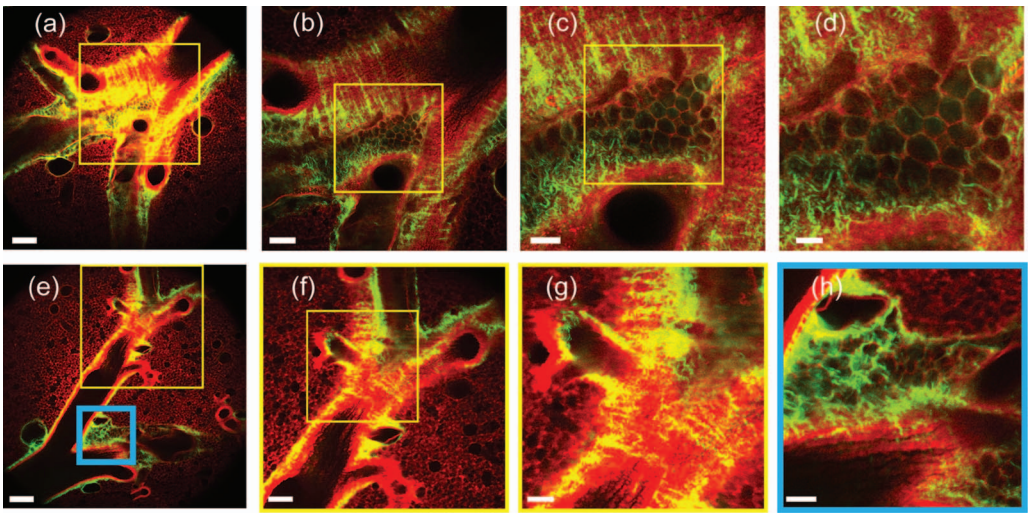

Fig. 2 Images of mouse lung. (a) and (e) Intrinsic fluorescence from elastin (red) and second-harmonic generation from collagen (green) in the lung imaged $\sim$1.4 mm below the surface. (Scale bars=200 μm.) (b) to (d) Digital zooms of the original, 4096$\times$4096 image in (a) as marked by yellow boxes. [Scale bars=100 μm, 50 μm, and 25 μm for (b) to (d), respectively.] (f) and (g) Digital zooms of the original, 4096$\times$4096 image in (e) as marked by yellow boxes. [Scale bars=100 μm, 50 μm, for (f) and (g), respectively.](h) Digital zoom of the original, 4096$\times$4096 image in (a) as marked by the blue box. (Scale bar=50 μm.)

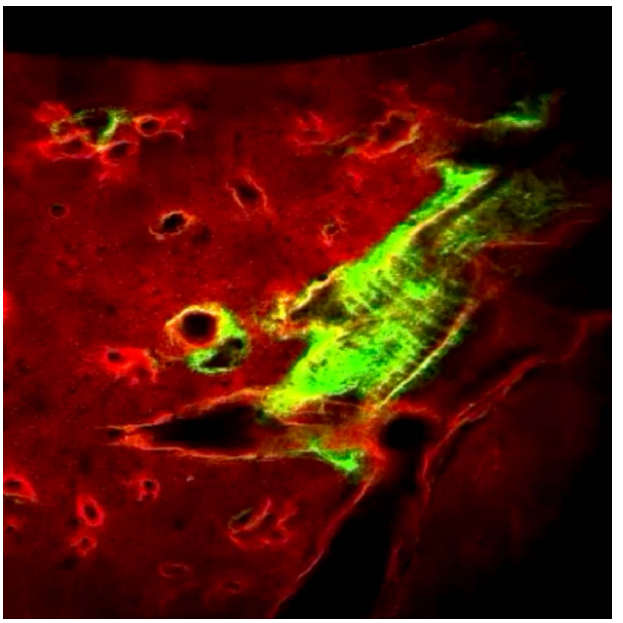

Video 2 Z-stack spanning 2.2 mm deep into the mouse lung. Each image is a 5-μm step in the z direction. Intrinsic fluorescence is in red, and second-harmonic generation from collagen is in green (QuickTime, 3.2 MB). [URL: http://dx.doi.org/10.1117/1.3454391.2]. (Color online only.)

Images of the brain taken ~850 μm from the top surface of the brain show the deeper cortical layers and the hippocampus (Fig. 4). The clearly delineated cells in the cortex are likely astrocytes, which have increased levels of cytosolic NADH.[14] The cell layer of the hippocampus is visible by the dark nuclei, which lack sources of intrinsic fluorescence. The dense white matter in the center of the brain prevented complete clearing of the tissue, ultimately limiting the depth of imaging.

The broad emission and absorption spectra of intrinsically fluorescent species complicates attempts to identify the molecular source. It is well known that the fixation process increases the brightness of intrinsic fluorescence, likely by decreasing nonradiative rates. In order to test whether new fluorescent species were being created by the fixation process, we measured the fluorescence spectrum from cleared brain tissue. The emission spectrum of the optically cleared brain matched that of live brain slice reported in previous literature[15] (data not shown). In addition, no visible emission was observed from either the PFA fixative or BABB clearing solutions.

4 Conclusion

The images presented here demonstrate the advantages of MPM of cleared tissue and point to several powerful applications. We have focused primarily on intrinsic fluorescence both because it is an area where MPM has a distinct advantage and because of its relation to the broad interest in the development of "optical biopsy," in which pathological evaluation of tissue may be performed *in situ*. While many groups have been pursuing the goal of establishing various forms of optical endomicroscopy as an alternative to conventional histology,[16–18] in many cases, physicians will still be required to take biopsy samples as standard procedure for the foreseeable future. Development of a tool for high-resolution, 3-D data sets of tissue morphology that is compatible with conventional techniques may both ease the transition to the use of images based on intrinsic fluorescence and create a powerful new tool for visualizing the structure of tissue beyond the limits of traditional 2-D approaches. In addition, other uses of cleared tissue[4–6] have established its compatibility with extrinsic fluorophores, and thereby indicate the wide range of potential application of MPM of cleared tissue with its inher-

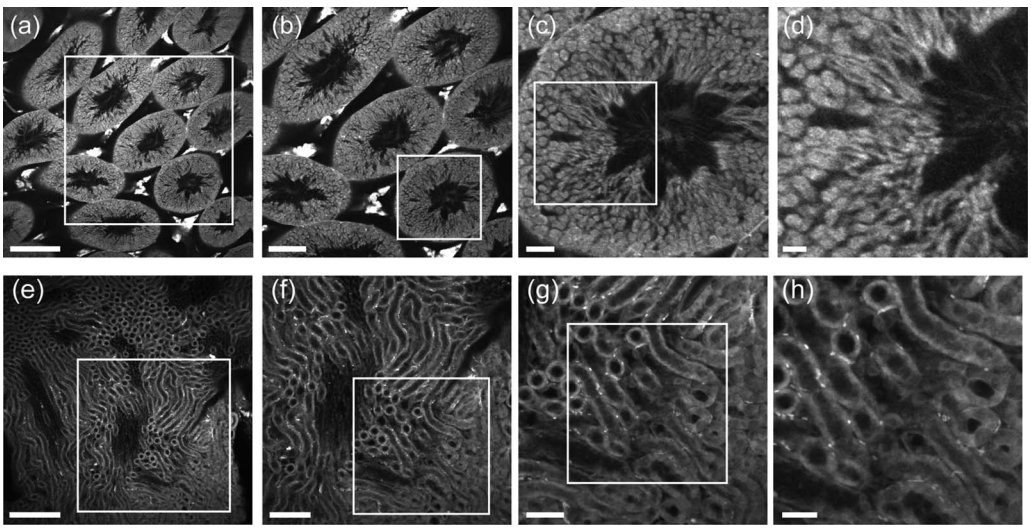

Fig. 3 Images of mouse testes and kidney. (a) Intrinsic fluorescence from testes imaged 1.4 mm from the surface. (Scale bar=200 μm.) (b) to (d) Digital zooms of the original, 4096×4096 image in (a) as marked by boxes. [Scale bars=100 μm, 25 μm, and 10 μm for (b) to (d), respectively.] (e) Intrinsic fluorescence from kidney imaged 1.1 mm from the surface. (Scale bar=200 μm.) (f) to (h) Digital zooms of the original, 4096 ×4096 image in (e) as marked by boxes. [Scale bars=100 μm, 50 μm, and 25 μm for (f) to (h), respectively.]

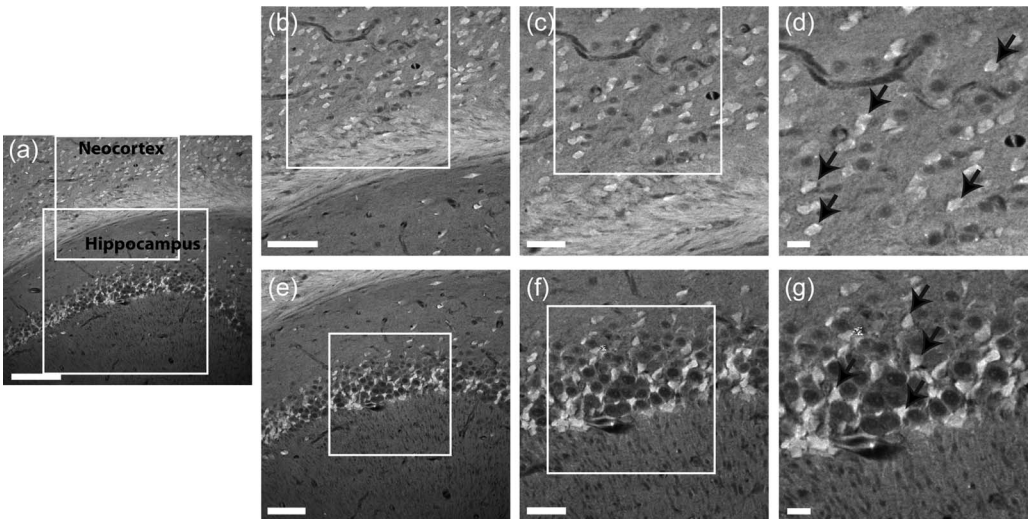

Fig. 4 Images of mouse brain. (a) Intrinsic fluorescence from brain taken 850 μm from the top surface showing lower regions of cortex and part of the hippocampus. (Scale bar=100 μm.) (b) to (d) Digital zooms of the cortex from the original, 4096×4096 image in (a) as marked by boxes. [Scale bars=50 μm, 25 μm, and 10 μm for (b) to (d), respectively.] (e) to (g) Digital zooms of the hippocampus from the original, 4096×4096 image in (a) as marked by boxes. [Scale bars=50 μm, 25 μm, and 10 μm for (e) to (g), respectively.] Astrocytes distinguished by their bright and uniform fluorescence signal are indicated by arrows in (d) and (g). Neuronal cell bodies are visible as dark spots in the cell layer of the hippocampus in (a) and (e) to (g).

ent advantages, including a very large field of view, limited only by the available optics, and flexibility in the pixel format, with images here as large as 4096×4096 pixels.

Acknowledgments

The authors want to acknowledge Dr. Richard Torres for advice and for providing comments on the manuscript and Eben Olson for his assistance witht he imaging software.

References

1. R. Cicchi, F. S. Pavone, D. Massi, and D. D. Sampson, "Contrast and depth enhancement in two-photon microscopy of human skin *ex vivo* by use of optical clearing agents," *Opt. Express* **13**(7), 2337–2344 (2005).
2. V. V. Tuchin, "A clear vision for laser diagnostics," *IEEE J. Sel. Top. Quantum Electron.* **13**(6), 1621–1628 (2007).
3. W. Spalteholz, *Uber das Durchsichtigmachen von menschlichen und tierischen Praparaten (About the transparency of human and animal preparations)*, S. Hierzal (1914).
4. J. A. Dent, A. G. Polson, and M. W. Klymkowsky, "A whole-mount immunocytochemical analysis of the expression of the intermediate filament protein vimentin in Xenopus," *Development* **105**, 61–74 (1989).
5. R. M. Zucker, "Whole insect and mammalian embryo imaging with confocal microscopy: morphology and apoptosis," *Cytometry, Part A* **69**(11), 1143–1152 (2006).
6. H. U. Dodt et al., "Ultramicroscopy: three-dimensional visualization of neuronal networks in the whole mouse brain," *Nat. Methods* **4**(4), 331–336 (2007).
7. J. Huisken, J. Swoger, F. Del Bene, J. Wittbrodt, and E. H. K. Stelzer, "Optical sectioning deep inside live embryos by selective plane illumination microscopy," *Science* **305**(5686), 1007–1009 (2004).
8. W. Denk, J. H. Strickler, and W. W. Webb, "2-photon laser scanning fluorescence microscopy," *Science* **248**(4951), 73–76 (1990).
9. W. R. Zipfel, R. M. Williams, and W. W. Webb, "Nonlinear magic: multiphoton microscopy in the biosciences," *Nat. Biotechnol.* **21**(11), 1369–1377 (2003).
10. W. R. Zipfel, R. M. Williams, R. Christie, A. Y. Nikitin, B. T. Hyman, and W. W. Webb, "Live tissue intrinsic emission microscopy using multiphoton-excited native fluorescence and second harmonic generation," *Proc. Natl. Acad. Sci. U.S.A.* **100**(12), 7075–7080 (2003).
11. T. Ragan, J. D. Sylvan, and K. H. Kim, "High-resolution whole organ imaging using two-photon tissue cytometry," *J. Biomed. Opt.* **12**, 014015 (2007).
12. P. S. Tsai et al., "All-optical histology using ultrashort laser pulses," *Neuron* **39**(1), 27–41 (2003).
13. T. A. Pologruto, B. L. Sabatini, and K. Svoboda, "ScanImage: flexible software for operating laser scanning microscopes," *Biomed. Eng. Online* **2** (2003), www.biomedical-engineering-online.com/content/2/1/13.
14. T. H. Chia, A. Williamson, D. D. Spencer, and M. J. Levene, "Multiphoton fluorescence lifetime imaging of intrinsic fluorescence in human and rat brain tissue reveals spatially distinct NADH binding," *Opt. Express* **16**(6), 4237–4249 (2008).
15. K. A. Kasischke, H. D. Vishwasrao, P. J. Fisher, W. R. Zipfel, and W. W. Webb, "Neural activity triggers neuronal oxidative metabolism followed by astrocytic glycolysis," *Science* **305**(5680), 99–103 (2004).
16. J. G. Fujimoto, C. Pitris, S. A. Boppart, and M. E. Brezinski, "Optical coherence tomography: an emerging technology for biomedical imaging and optical biopsy," *Neoplasia* **2**(1–2), 9–25 (2000).
17. K. Konig and I. Riemann, "High-resolution multiphoton tomography of human skin with subcellular spatial resolution and picosecond time resolution," *J. Biomed. Opt.* **8**(432), 432–439 (2003).
18. M. C. Pierce, D. J. Javier, and R. Richards-Kortum, "Optical contrast agents and imaging systems for detection and diagnosis of cancer," *Int. J. Cancer* **123**, 1979–1990 (2008).